Red blood cell metabolism in Rhesus macaques and humans: comparative biology of blood storage

Davide Stefanoni,[1] Hye Kyung H. Shin,[2] Jin Hyen Baek,[2] Devin P. Champagne,[1] Travis Nemkov,[1] Tiffany Thomas,[3] Richard O. Francis,[3] James C. Zimring,[4] Tatsuro Yoshida,[5] Julie A. Reisz,[1] Steven L. Spitalnik,[3] Paul W. Buehler[2] and Angelo D'Alessandro[1,6]

[1]Department of Biochemistry and Molecular Genetics, University of Colorado Denver – Anschutz Medical Campus, Aurora, CO; [2]Center for Biologics Evaluation and Research, Food and Drug Administration, Silver Spring, MD; [3]Department of Pathology & Cell Biology, Columbia University, New York, NY; [4]BloodWorks Northwest, Seattle, WA; [5]Hemanext Inc, Lexington, MA and [6]Department of Medicine, Division of Hematology, University of Colorado Denver – Anschutz Medical Campus, Aurora, CO, USA

©2020 Ferrata Storti Foundation. This is an open-access paper. doi:10.3324/haematol.2019.229930

Received: June 19, 2019.

Accepted: October 10, 2019.

Pre-published: November 7, 2019.

Correspondence: *ANGELO D'ALESSANDRO* - angelo.dalessandro@ucdenver.edu

PAUL W. BUEHLER - Paul.Buehler@fda.hhs.gov

SUPPLEMENTARY MATERIAL

TABLE OF CONTENTS

SUPPLEMENTARY METHODS - EXTENDED

Blood collection: Blood was collected into a syringe using a 20 G needle from the femoral vein of five-year-old rhesus macaques (n=20; 10 male/10 female) under ketamine/dexmedotomidine (7 mg/kg/0.2 mg/kg, intramuscular) anesthesia according to FDA White Oak animal care and use protocol 2018-31. All blood donor animals originated from the same colony located at Morgan Island, South Carolina and were naïve to experimentation at the time of blood collection. Blood was collected into a syringe using a 16 G needle from the median cubital vein of 30-75-year-old human volunteers (n=21; 11 male/10 female) under informed consent according to NIH study IRB #99-CC-0168 "Collection and Distribution of Blood Components from Healthy Donors for In Vitro Research Use" under an NIH-FDA material transfer agreement.

Blood processing: To maintain consistency across comparisons, rhesus macaque and human blood was collected, processed, stored, and sampled the same way. Whole blood was collected in syringes into acid citrate dextrose solution A (Becton Dickenson, Franklin Lakes, NJ USA) to make up 15% of the volume. Collected blood was individually processed by passage through a pediatric leukoreduction filter (Haemonetics, Braintree, MA USA). Approximately 20 ml of leukoreduced whole blood was then centrifuged at 2,000 rpm for 10 minutes, plasma was removed, and 0.45 ml of AS-3 (Haemonetics, Braintree, MA USA) was added for every 1 ml of packed RBCs. The RBCs in AS-3 preservative solution (total volume ~12-15 ml) were transferred to a sterile customized single port bag through a sterile self-sealing sampling site coupler port (Fenwal, Lake Zurich, IL USA). The volume modified storage bags (Hemanext Inc., Lexington, MA USA), were designed to hold 20 ml volumes and mimicked the composition of standard full-sized units (i.e., incorporating polyvinylchloride (PVC) and phthalate plasticizers). All processing procedures were performed in a biosafety cabinet under aseptic conditions the morning of the blood collections.

RBC storage and sampling: RBCs were stored at 4-6ºC for 42 days. Sampling was performed in a biosafety cabinet, by obtaining 500 µL from each unit using a 16G/1-inch needle and 1 ml syringe after thorough mixing of each bag. Collections were performed on days 0, 7, 14,

21, 28, 35, and 42. Samples were centrifuged at 2,500 rpm for 10 minutes at 4ºC, separated into supernatant and RBCs for each time point, and stored at -80ºC until analysis.

Sample processing and metabolite extraction: A volume of 50 µL of frozen RBC aliquots was extracted 1:10 in ice cold extraction solution (methanol:acetonitrile:water 5:3:2 *v/v*).[1] Samples were vortexed and insoluble material pelleted, as described.[2,3] For lipidomics analyses, supernatants were diluted 1:1 (v/v) with 10 mM ammonium acetate for analysis by ultra-high pressure liquid chromatography coupled to mass spectrometry (UHPLC-MS).

Ultra-High-Pressure Liquid Chromatography-Mass Spectrometry (MS) metabolomics: The analytical platform employs a Vanquish UHPLC system (Thermo Fisher Scientific, San Jose, CA, USA) coupled online to a Q Exactive mass spectrometer (Thermo Fisher Scientific, San Jose, CA, USA).

Metabolomics: UHPLC-MS metabolomics analyses were performed using a Vanquish UHPLC system coupled online to a high-resolution Q Exactive mass spectrometer (Thermo Fisher, Bremen, Germany). Samples were resolved over a Kinetex C18 column (2.1x150 mm, 1.7 µm; Phenomenex, Torrance, CA, USA) at 45°C. A volume of 10 ul of sample extracts was injected into the UHPLC-MS. Each sample was injected and run four times with two different chromatographic and MS conditions as follows: 1) using a 5 minute gradient at 450 µL/minute from 5-95% B (A: water/0.1% formic acid; B:acetonitrile/0.1% formic acid) and the MS was operated in positive mode and 2) using a 5 minute gradient at 450 µL/minute from 5-95% B (A: 5% acetonitrile, 95%water/1 mM ammonium acetate; B:95%acetonitrile/5% water, 1 mM ammonium acetate) and the MS was operated in negative ion mode. The UHPLC system was coupled online with a Q Exactive (Thermo, San Jose, CA, USA) scanning in Full MS mode at 70,000 resolution in the 60-900 m/z range, 4 kV spray voltage, 15 sheath gas and 5 auxiliary gas, operated in negative or positive ion mode (separate runs). These chromatographic and MS conditions were applied for both relative and targeted quantitative metabolomics measurements, with the differences that for the latter targeted quantitative post hoc analyses were performed on the basis of the stable isotope-labeled internal standards used as a reference quantitative measurement, as detailed below.

Lipidomic:s Samples were resolved over an ACQUITY HSS T3 column (2.1 x 150 mm, 1.8 µm particle size (Waters, MA, USA) using an aqueous phase (A) of 25% acetonitrile and 5 mM ammonium acetate and a mobile phase (B) of 50% isopropanol, 45% acetonitrile and 5 mM ammonium acetate. Samples were eluted from the column using either the solvent gradient: 0-1 min 25% B and 0.3 mL/min; 1-2 min 25-50% B and 0.3 mL/min, 2-8 min 50-90% B and 0.3 mL/min, 8-10 min 90-99% B and 0.3 mL/min, 10-14 min hold at 99% B and 0.3 mL/min, 14-14.1 min 99-25% B 1and 0.3 mL/min, 14.1-16.9 min hold at 25% B and 0.4 mL/min, 16.9-17 min hold at 25% B and resume flow of 0.3 mL/min. isocratic elution of 5% B flowed at 250 µl/min and 25ºC or a gradient from 0- 5% B over 0.5 min; 5-95% B over 0.6 min, hold at 95% B for 1.65 min; 95-5% B over 0.25 min; hold at 5% B for 2 min, flowed at 450 µl/min and 35ºC[4]. The Q Exactive mass spectrometer (Thermo Fisher Scientific, San Jose, CA, USA) was operated independently in positive or negative ion mode, scanning in Full MS mode (2 µscans) from 150 to 1500 m/z at 70,000 resolution, with 4 kV spray voltage, 45 shealth gas, 15 auxiliary gas. When required, dd-MS2 was performed at 17,500 resolution, AGC target = 1e5, maximum IT = 50 ms, and stepped NCE of 25, 35 for positive mode, and 20, 24, and 28 for negative mode.

Quality control and data processing: Calibration was performed prior to analysis using the Pierce™ Positive and Negative Ion Calibration Solutions (Thermo Fisher Scientific). Acquired data was then converted from .raw to .mzXML file format using Mass Matrix (Cleveland, OH, USA). Samples were analyzed in randomized order with a technical mixture injected incrementally to qualify instrument performance. This technical mixture was also injected three times per polarity mode and analyzed with the parameters above, except CID fragmentation was included for unknown compound identification.

Metabolite assignment and relative quantitation: Metabolite assignments, isotopologue distributions, and correction for expected natural abundances of deuterium, ^{13}C, and ^{15}N isotopes were performed using MAVEN (Princeton, NJ, USA),[5] against an in house library of deuterated lipid standards (SPLASH® LIPIDOMIX® Mass Spec Standard, Avanti Lipids). Discovery mode analysis was performed with standard workflows using Compound Discoverer (Thermo Fisher Scientific, San Jose, CA). From these analyses, follow up elaboration for untargeted metabolomics results were performed only the top 10,000 unique chemical formulae upon sorting on relative

abundance (peak areas – arbitrary units), as determined from high-resolution accurate intact mass, isotopic pattern, and MS^2 fragmentation spectra against the KEGG pathway, HMDB, ChEBI, and ChEMBL databases. Additional analyses, including untargeted lipidomics via LipidSearch (Thermo Fisher, Bremen, Germany). Graphs and statistical analyses (either t-test or repeated measures ANOVA) were prepared with GraphPad Prism 5.0 (GraphPad Software, Inc, La Jolla, CA), GENE E (Broad Institute, Cambridge, MA, USA), and MetaboAnalyst 4.0.[6]

Targeted quantitative metabolomics: Targeted quantitative metabolomics analyses were performed on all RBC and supernatant samples from fresh and stored human and RM RBCs. All the samples were extracted with the exact same protocol detailed above. However, for this validation analysis, extraction solutions (methanol:acetonitrile:water 5:3:2 *v/v*) were supplemented with the following standards:

Metabolite	Labeling	Neutral Formula	MW	Vendor	Product ID	Final concentration (uM)
a-Ketoglutarate	13C5	*C5H6O5	151.05	Cambridge	CLM-2411-PK	1
Adenosine						1
Citric acid	2,2,4,4-D4	C6H4D4O7	196.15	Cambridge	DLM-3487-PK	1
Fumaric acid	1,4-13C2	*C2C2H4O4	118.05	Cambridge	CLM-4454-PK	1
Glutathione (GSH)	Gly13C2,15N	*C2C8H17*N1N2O6	310.3	Cambridge	CNLM-6245.50	10
Glucose	13C6	*C6H12O6	186.09	Cambridge	CLM-1396-1	10
Lactate	1-13C	*C1C2H6O3	113.05	Cambridge	CLM-1577-1	40
Palmitic acid	U-13C16	*C16H32O2	272.25	Cambridge	CLM-409-0.5	1
Sphingosine 1P	D7	C18H31D7NO5P	386.51	Avanti	860659-1MG	0.5
Succinic acid	13C x 4	*C4H6O4	122.05	Cambridge	CLM-1571-0.25	1
AA Mix (including the standards below)				Cambridge	MSK-A2-1.2	1
L-Alanine	13C3, 15N	*C3H7*NO2				1
L-Arginine:HCl	13C6, 15N4	*C6H15Cl*N4O2 (isotopic *C6H14*N4O2)				1
L-Aspartic acid	13C4, 15N	*C4H7*NO4				1
L-Cystine	13C6, 15N2	*C6H12*N2O4S2				1
L-Glutamic acid	13C5, 15N	*C5H9*NO4				1
Glycine	13C2, 15N	*C2H5*NO2				1
L-Histidine:HCl:H2O	13C6, 15N3	*C6H12Cl*N3O3 (isotopic *C6H9*N3O2)				1
L-Isoleucine	13C6, 15N	*C6H13*NO2				1
L-Leucine	13C6, 15N	*C6H13*NO2				1
L-Lysine:2HCl	13C6, 15N2	*C6H16Cl2*N2O2 (isotopic *C6H14*N2O2)				1
L-Methionine	13C5, 15N	*C5H11*NO2S				1
L-Phenylalanine	13C9, 15N	*C9H11*NO2				1
L-Proline	13C5, 15N	*C5H9*NO2				1
L-Serine	13C3, 15N	*C3H7*NO3				1
L-Threonine	13C4, 15N	*C4H9*NO3				1
L-Tyrosine	13C9, 15N	*C9H11*NO3				1
L-Valine	13C5, 15N	*C5H11*NO2				1

Samples were processed with the same UHPLC-MS setup described above. However, upon acquisition, raw data were converted to .mzxml and peak areas for light and heavy (stable isotope-labeled) isotopologues were exported for each metabolite, as extensively described in prior methodological work[4,7,8]. In details, absolute concentrations were determined using the following formula: [light] = (abundance light) / (abundance heavy) * [heavy] [dilution factor] where [light] = concentration of non-isotopic metabolite, (abundance light) = total area abundance of non-isotopic metabolite, (abundance heavy) = total area abundance of isotopic metabolite, and [heavy] = known concentration isotopic metabolite.

SUPPLEMENTARY DISCUSSION

Red blood cells (RBCs) are the most abundant cell type in humans (~83% of the total cells in adult humans)[9]. All vertebrates, except for cold-water ice fish, transport oxygen via RBC hemoglobin, making RBCs a centerpiece in the evolution of the vertebrate circulatory system.[10] However, across vertebrates, RBCs vary in size (up to thirtyfold[10]), lifespan,[11–13] and organelle[14] and protein content.[15] In humans, mature RBCs have an average diameter of ~6.2-8.2 µm and a thickness of ~0.8-1 µm, due to their discocytic shape resulting from the loss of organelles (e.g., nuclei, mitochondria, ribosomes) during differentiation. To transport and deliver oxygen to tissues, mature RBCs are loaded with hemoglobin (~250-270 million copies/cell,[16] ~90% of the total protein content of mature RBCs). However, globin sequence variation across vertebrates is significant,[17] as is hemoglobin's capacity for carrying and delivering oxygen in mammals adapted to extreme conditions, such as winter hibernators.[18] Despite their apparent simplicity, human RBCs exhibit a complex proteome, comprising ~3,000 proteins[19–21] with complex structural and enzymatic functions. Therefore, despite their lack of mitochondria and other organelles, our current understanding of the complexity of RBC metabolism exceeds that described in classical studies. For example, historically, RBC metabolism was thought to rely exclusively on glucose oxidation as the main source of reducing equivalents (e.g., NADPH via the pentose phosphate pathway (PPP)) and high-energy phosphate compounds, either via the Embden-Meyerhof-Parnas glycolytic pathway (e.g., for adenosine triphosphate (ATP)) or the Rapoport-Luebering shunt (e.g., for 2,3-diphosphoglycerate (DPG)). Nonetheless, it is now clear that RBC metabolism also involves a complex interplay of cytosolic isoforms of Krebs cycle enzymes, which may play a role in the homeostasis of reducing equivalents,[22] purine oxidation and salvage reactions,[23] carnitine-dependent[24] and -independent lipid recycling[25] and sphingolipid metabolism,[26] arginine metabolism and the potential generation of nitric oxide through nitric oxide synthase[27] and arginase,[28] and one-carbon and sulfur metabolism involved in recycling oxidized proteins.[29,30] In addition, RBCs express at least 77 small molecule transporters,[31] which makes the analysis of RBC metabolism a window into systems-wide or organ-specific metabolic dysfunction achievable by peripheral blood sampling[32]. As such, investigating RBC metabolism is not only relevant *per se*, but also provides clues into system metabolism.

In the present study, we provide a comprehensive targeted and untargeted metabolomics and lipidomics description of RBCs from humans and RMs – further validated with tracing

experiments and quantitative measurements against stable isotope-labeled internal standards. Overall, there was substantial inter-species overlap in the metabolic changes occurring during refrigerated storage, although species-specific differences were identified with respect to the rate and extent to which some of these changes occur. Specifically, there were significant increases in glutathione and sulfur metabolism in RMs, accompanied by increased purine and lipid oxidation; the latter are negative predictors of post-transfusion RBC recovery in mice and humans[31,35]. In addition, higher levels of plasticizers, fatty acyl-carnitine metabolism, and PS content were found, all of which are markers consistent with increased lipid remodeling and the (slightly) shorter lifespan of RM, as compared to human, RBCs. Sex and species-specific alterations of arginine and carboxylic acid/transamination metabolism were also found, suggesting potential confounders when using RM RBCs to study nitric oxide/polyamine metabolism and reducing equivalents.

In brief, the results reported in this study could serve as a reference for follow-up studies on human RBC storage metabolism, as well as RM RBC biology or as a comparative dataset for future transfusion medicine studies focusing on non-human primates or other animal models.

SUPPLEMENTARY REFERENCES

1. Reisz JA, Nemkov T, Dzieciatkowska M, Culp-Hill R, Stefanoni D, Hill RC, et al. Methylation of protein aspartates and deamidated asparagines as a function of blood bank storage and oxidative stress in human red blood cells. Transfusion (Paris). 2018 Dec;58(12):2978–91.
2. Nemkov T, Hansen KC, Dumont LJ, D'Alessandro A. Metabolomics in transfusion medicine. Transfusion (Paris). 2016 Apr;56(4):980–93.
3. D'Alessandro A, Nemkov T, Yoshida T, Bordbar A, Palsson BO, Hansen KC. Citrate metabolism in red blood cells stored in additive solution-3. Transfusion (Paris). 2017 Feb;57(2):325–36.
4. Reisz JA, Zheng C, D'Alessandro A, Nemkov T. Untargeted and Semi-targeted Lipid Analysis of Biological Samples Using Mass Spectrometry-Based Metabolomics. Methods Mol Biol Clifton NJ. 2019;1978:121–35.
5. Melamud E, Vastag L, Rabinowitz JD. Metabolomic Analysis and Visualization Engine for LC−MS Data. Anal Chem. 2010 Dec;82(23):9818–26.
6. Chong J, Soufan O, Li C, Caraus I, Li S, Bourque G, et al. MetaboAnalyst 4.0: towards more transparent and integrative metabolomics analysis. Nucleic Acids Res. 2018 Jul 2;46(W1):W486–94.
7. Nemkov T, Hansen KC, D'Alessandro A. A three-minute method for high-throughput quantitative metabolomics and quantitative tracing experiments of central carbon and nitrogen pathways. Rapid Commun Mass Spectrom RCM. 2017 Apr 30;31(8):663–73.
8. Nemkov T, Reisz JA, Gehrke S, Hansen KC, D'Alessandro A. High-Throughput Metabolomics: Isocratic and Gradient Mass Spectrometry-Based Methods. Methods Mol Biol Clifton NJ. 2019;1978:13–26.
9. Bianconi E, Piovesan A, Facchin F, Beraudi A, Casadei R, Frabetti F, et al. An estimation of the number of cells in the human body. Ann Hum Biol. 2013 Dec;40(6):463–71.
10. Snyder GK, Sheafor BA. Red Blood Cells: Centerpiece in the Evolution of the Vertebrate Circulatory System. Integr Comp Biol. 1999 Apr 1;39(2):189–98.
11. Franco RS. Measurement of Red Cell Lifespan and Aging. Transfus Med Hemotherapy. 2012 Oct;39(5):302–7.
12. Rodnan GP, Ebaugh FG, Fox MRS. The life span of the red blood cell and the red blood cell volume in the chicken, pigeon and duck as estimated by the use of Na2Cr51O4, with observations on red cell turnover rate in the mammal, bird and reptile. Blood. 1957 Apr;12(4):355–66.
13. Kaestner L, Minetti G. The potential of erythrocytes as cellular aging models. Cell Death Differ. 2017 Sep;24(9):1475–7.
14. Moras M, Lefevre SD, Ostuni MA. From Erythroblasts to Mature Red Blood Cells: Organelle Clearance in Mammals. Front Physiol [Internet]. 2017 Dec 19 [cited 2019 May 7];8. Available from: https://www.ncbi.nlm.nih.gov/pmc/articles/PMC5742207/
15. Pasini EM, Kirkegaard M, Mortensen P, Mann M, Thomas AW. Deep-coverage rhesus red blood cell proteome: a first comparison with the human and mouse red blood cell. Blood Transfus. 2010 Jun;8(Suppl 3):s126–39.
16. Bryk AH, Wiśniewski JR. Quantitative Analysis of Human Red Blood Cell Proteome. J Proteome Res. 2017 Aug 4;16(8):2752–61.
17. Götting M, Nikinmaa M. More than hemoglobin – the unexpected diversity of globins in vertebrate red blood cells. Physiol Rep [Internet]. 2015 Feb 3 [cited 2019 May 7];3(2). Available from: https://www.ncbi.nlm.nih.gov/pmc/articles/PMC4393193/
18. Revsbech IG, Fago A. Regulation of blood oxygen transport in hibernating mammals. J Comp Physiol [B]. 2017 Jul;187(5–6):847–56.
19. D'Alessandro A, Dzieciatkowska M, Nemkov T, Hansen KC. Red blood cell proteomics update: is there more to discover? Blood Transfus. 2017 Mar;15(2):182–7.
20. Gautier E-F, Leduc M, Cochet S, Bailly K, Lacombe C, Mohandas N, et al. Absolute proteome quantification of highly purified populations of circulating reticulocytes and mature erythrocytes. Blood Adv. 2018 Oct 23;2(20):2646–57.
21. Wilson MC, Trakarnsanga K, Heesom KJ, Cogan N, Green C, Toye AM, et al. Comparison of the proteome of adult and cord erythroid cells, and changes in the proteome following reticulocyte maturation. Mol Cell Proteomics. 2016 Jan 1;mcp.M115.057315.
22. Nemkov T, Sun K, Reisz JA, Yoshida T, Dunham A, Wen EY, et al. Metabolism of Citrate and Other Carboxylic Acids in Erythrocytes As a Function of Oxygen Saturation and Refrigerated Storage. Front Med. 2017;4:175.
23. Nemkov T, Sun K, Reisz JA, Song A, Yoshida T, Dunham A, et al. Hypoxia modulates the purine salvage pathway and decreases red blood cell and supernatant levels of hypoxanthine during refrigerated storage. Haematologica. 2018 Feb;103(2):361–72.

24. Nikolaos S, George A, Telemachos T, Maria S, Yannis M, Konstantinos M. Effect of L-carnitine supplementation on red blood cells deformability in hemodialysis patients. Ren Fail. 2000 Jan;22(1):73–80.
25. Wu H, Bogdanov M, Zhang Y, Sun K, Zhao S, Song A, et al. Hypoxia-mediated impaired erythrocyte Lands' Cycle is pathogenic for sickle cell disease. Sci Rep [Internet]. 2016 Jul 20 [cited 2019 May 7];6. Available from: https://www.ncbi.nlm.nih.gov/pmc/articles/PMC4951653/
26. Sun K, Zhang Y, D'Alessandro A, Nemkov T, Song A, Wu H, et al. Sphingosine-1-phosphate promotes erythrocyte glycolysis and oxygen release for adaptation to high-altitude hypoxia. Nat Commun. 2016 Jul 15;7:12086.
27. Kleinbongard P, Schulz R, Rassaf T, Lauer T, Dejam A, Jax T, et al. Red blood cells express a functional endothelial nitric oxide synthase. Blood. 2006 Apr 1;107(7):2943–51.
28. D'Alessandro A, Reisz JA, Zhang Y, Gehrke S, Alexander K, Kanias T, et al. Effects of aged stored autologous red blood cells on human plasma metabolome. Blood Adv. 2019 Mar 26;3(6):884–96.
29. Reisz JA, Nemkov T, Dzieciatkowska M, Culp-Hill R, Stefanoni D, Hill RC, et al. Methylation of protein aspartates and deamidated asparagines as a function of blood bank storage and oxidative stress in human red blood cells. Transfusion (Paris). 2018;
30. Barber JR, Clarke S. Membrane protein carboxyl methylation increases with human erythrocyte age. Evidence for an increase in the number of methylatable sites. J Biol Chem. 1983 Jan 25;258(2):1189–96.
31. Nemkov T, Reisz JA, Xia Y, Zimring JC, D'Alessandro A. Red blood cells as an organ? How deep omics characterization of the most abundant cell in the human body highlights other systemic metabolic functions beyond oxygen transport. Expert Rev Proteomics. 2018 Nov;15(11):855–64.
32. D'Alessandro A, Giardina B, Gevi F, Timperio AM, Zolla L. Clinical Metabolomics: the next stage of clinical biochemistry. Blood Transfus. 2012 May;10(Suppl 2):s19–24.
33. Fergusson DA, Hébert P, Hogan DL, LeBel L, Rouvinez-Bouali N, Smyth JA, et al. Effect of fresh red blood cell transfusions on clinical outcomes in premature, very low-birth-weight infants: the ARIPI randomized trial. JAMA. 2012 Oct 10;308(14):1443–51.
34. Steiner ME, Ness PM, Assmann SF, Triulzi DJ, Sloan SR, Delaney M, et al. Effects of red-cell storage duration on patients undergoing cardiac surgery. N Engl J Med. 2015 Apr 9;372(15):1419–29.
35. Heddle NM, Cook RJ, Arnold DM, Liu Y, Barty R, Crowther MA, et al. Effect of Short-Term vs. Long-Term Blood Storage on Mortality after Transfusion. N Engl J Med. 2016 17;375(20):1937–45.
36. DeSantis SM, Brown DW, Jones AR, Yamal J-M, Pittet J-F, Patel RP, et al. Characterizing red blood cell age exposure in massive transfusion therapy: the scalar age of blood index (SBI). Transfusion (Paris). 2019 May 3;
37. Francis RO, Mahajan S, Rapido F, La Carpia F, Soffing M, Divgi C, et al. Reexamination of the chromium-51-labeled posttransfusion red blood cell recovery method. Transfusion (Paris). 2019 Apr 19;

SUPPLEMENTARY FIGURES

Supplementary Figures

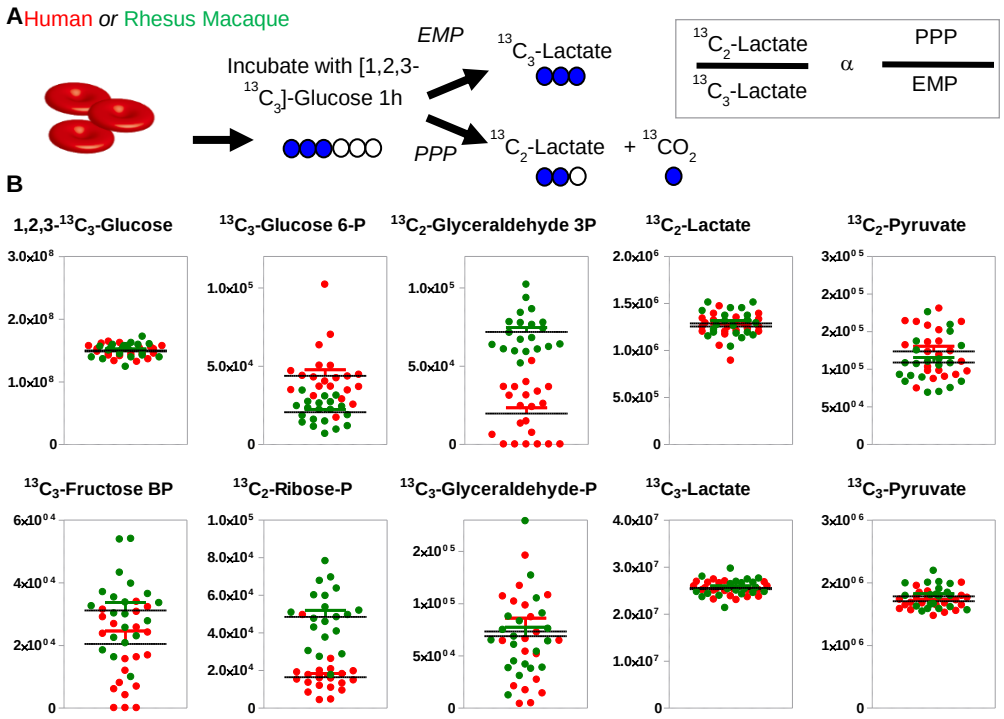

Supplementary Figure 1 – Metabolism of [1,2,3-$^{13}C_3$]glucose in human (red) or macaque (green) RBCs. The experimental schema is shown in **A**. Measurement of $^{13}C_2$-lactate vs $^{13}C_3$-lactate indicates glucose flux through the pentose phosphate pathway (PPP). In **B**, metabolites downstream of glucose in the glycolytic pathway and the PPP, particularly end-product lactate, indicate no observed differences between fresh human and RM RBCs following a 1 h incubation with [1,2,3-$^{13}C_3$]glucose. y-Axes are abundance (a.u.); RM RBCs in green and human RBCs in red.


Time
0
21
42
Species
H
RM
relative
row min
Species
Time
Ann

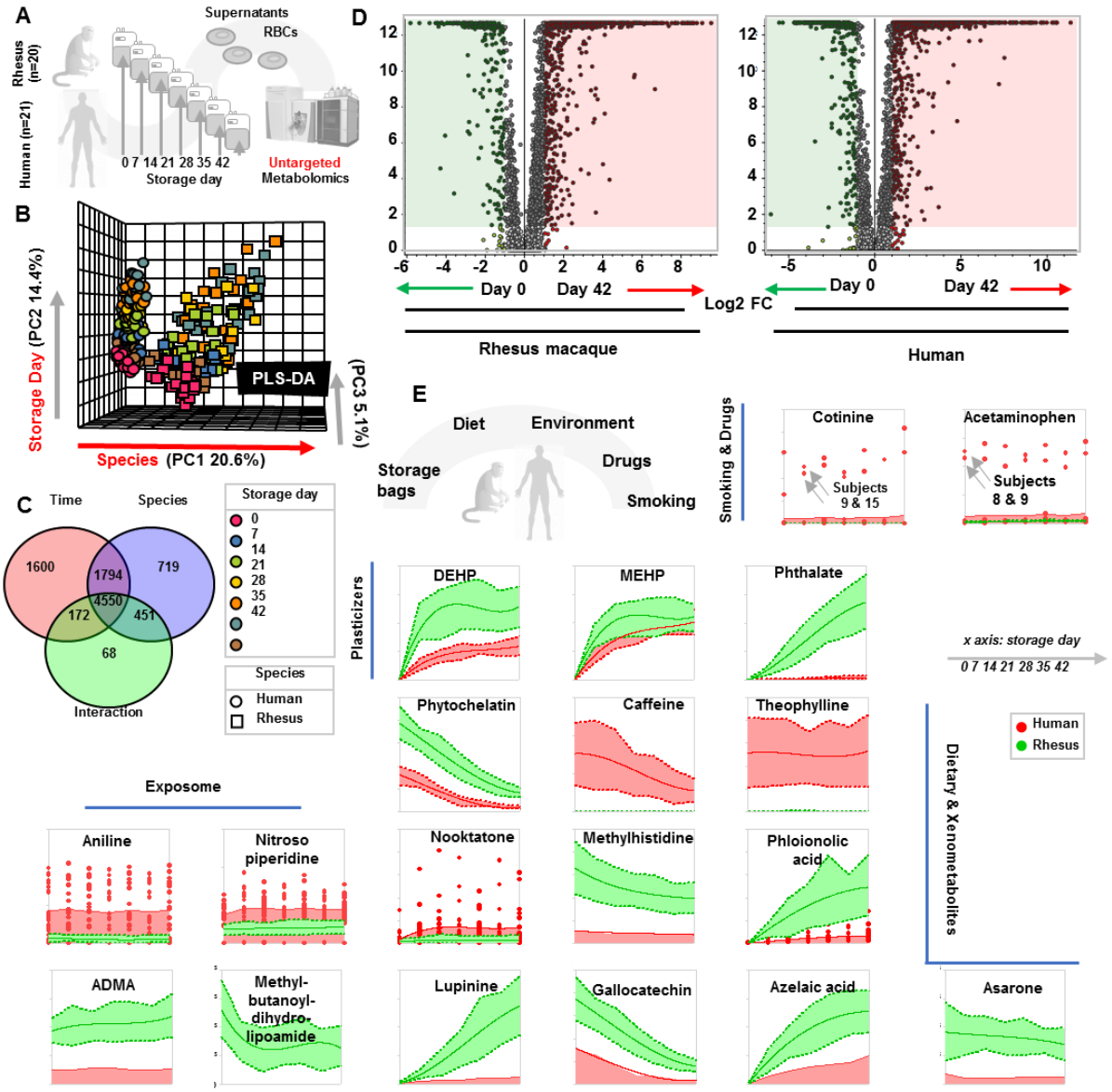

Supplementary Figure 3 – Untargeted metabolomics analyses of RBCs from humans (n=21) and rhesus macaques (n=20). The experimental schema is shown in **A**. PLS-DA (**B**), number of significant metabolites by ANOVA as a function of species and storage duration, or interaction of the factors (**C**), and volcano plots for day 42 vs. day 0 RBCs in RMs (left) and humans (right) are shown (**D**). In **E,** line plot highlights of metabolites derived from the plastic bags, dietary or other xenometabolites (from drugs, exposure to cigarette smoke, etc – RM RBCs in green and human RBCs in red).

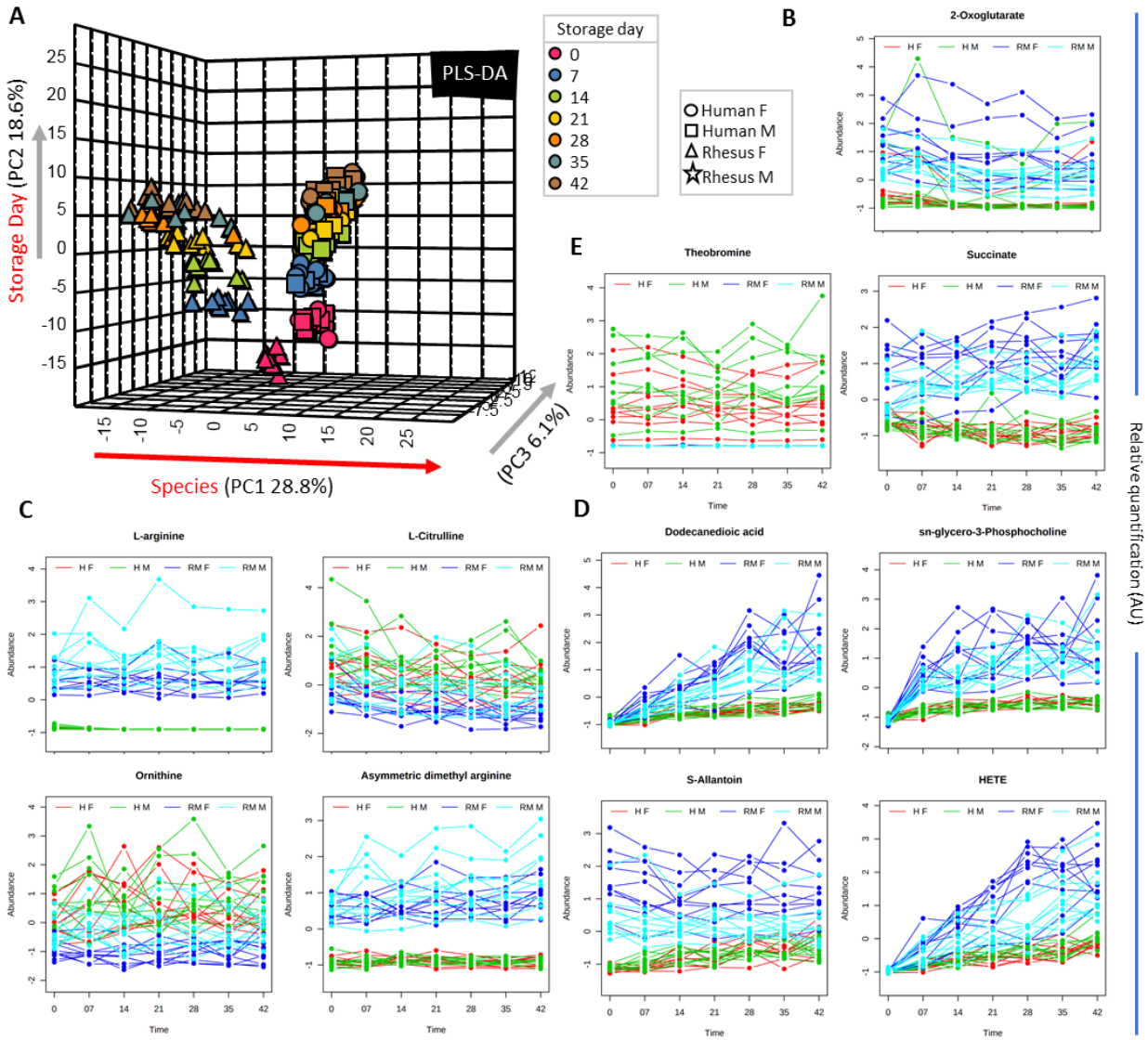

Supplementary Figure 4 – Species and storage had a higher impact on RBC metabolic phenotypes than sex. In **(A)**, species accounted for 28.8 and storage days for 18.6% of the differences, whereas sex only accounted for 6.1% of difference. However, sex had a significant impact on carboxylate metabolism (oxoglutarate and succinate) (**B**), arginine metabolism (**C**), and fatty acid oxidation (**D**). **→continues next page**

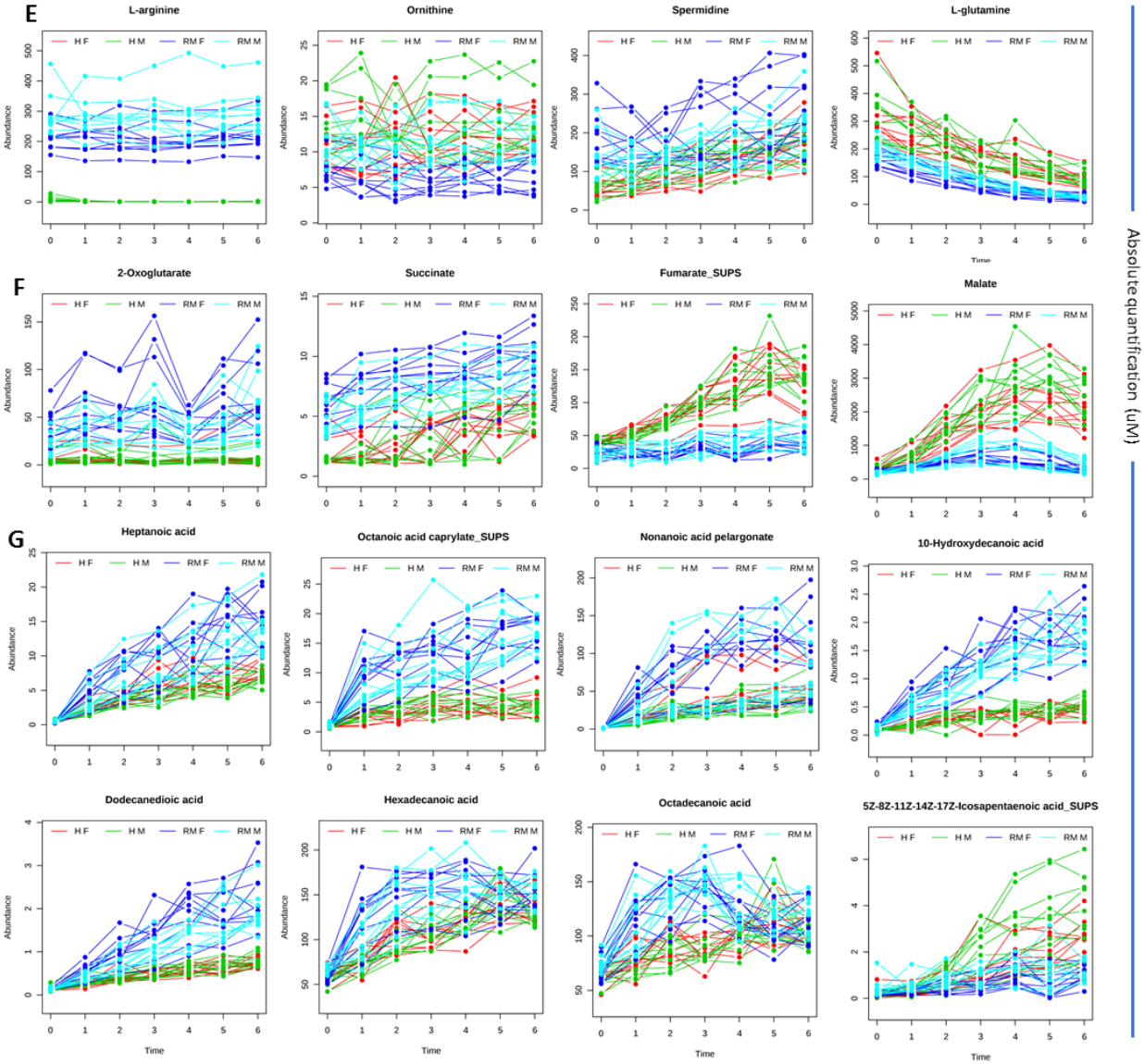

➔ **Continues from previous page Supplementary Figure 4 –** These results were validated via targeted quantitative measurements against stable isotope-labeled internal standards. In particular, we confirmed that arginine metabolites (**E**)**,** carboxylic acids (**F**), and free fatty acids (**G**) showed different storage-dependent abundances in humans and RM as a function of sex.

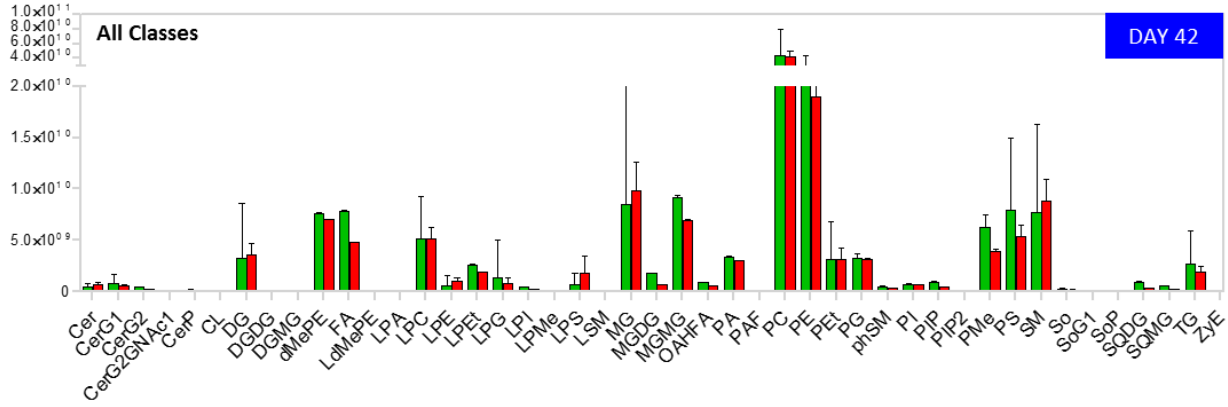

Supplementary Figure 5 – Bar graphs (Mean ± SD) of lipid classes at the end of storage in human (n=21; red) or rhesus macaque RBCs (n=20, green), calculated by the sum of all fatty-acyl groups in each class detected in each sample.

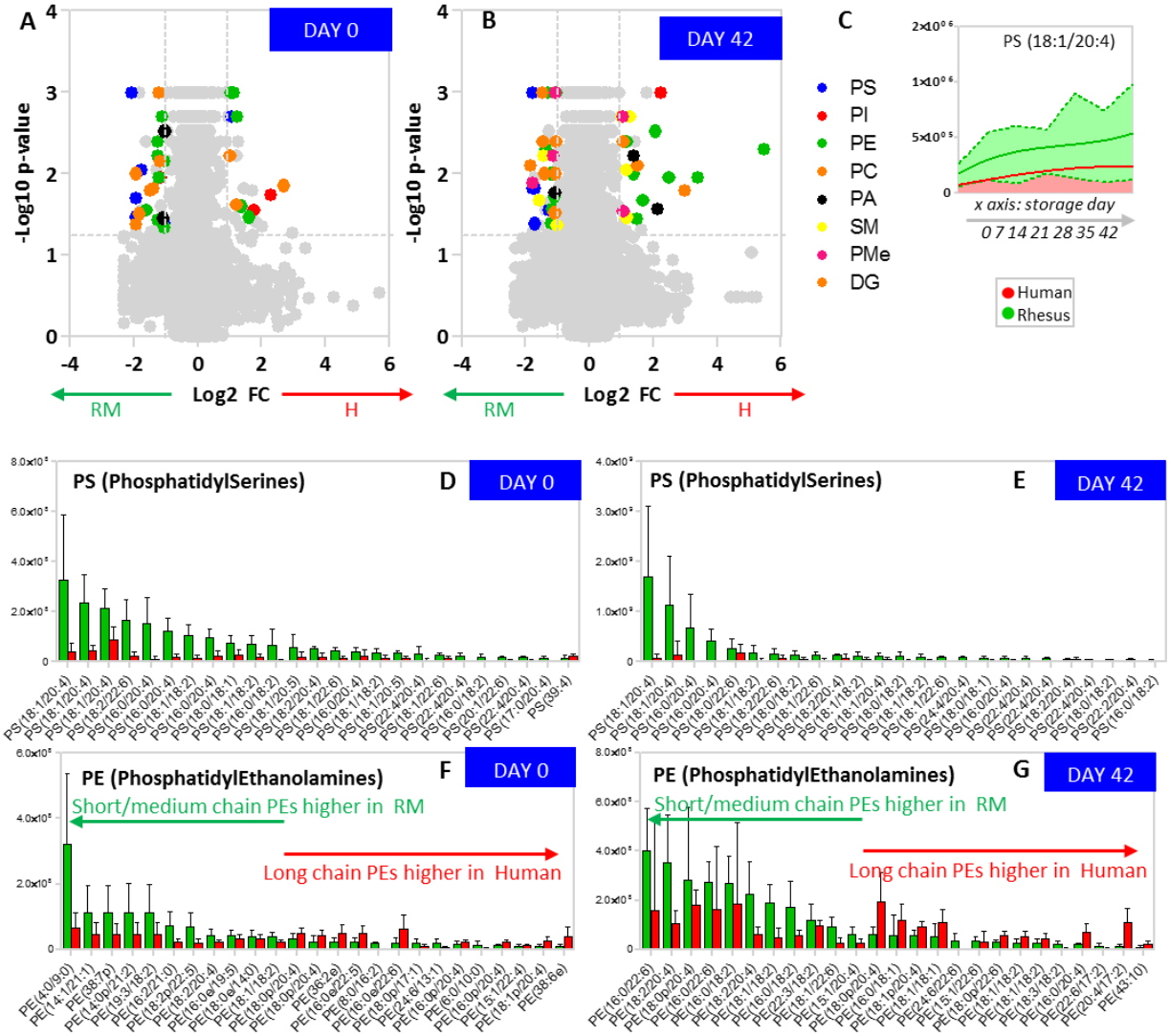

Supplementary Figure 6 – Lipidomics analyses of human (red) and rhesus macaque (green) RBCs at storage day 0 (A) and 42 (B). Significantly higher levels of phosphatidylserines – including PS (18:0/20:4 – **C**) were measured in RM RBCs at day 0 (**D**) and 42 (**E**). Higher levels of short and medium chain phosphatidylethanolamines (PEs), but not long chain PEs were detected in RM RBCs in comparison to day 0 (**F**) or 42 (**G**) human RBCs.

Time (week)
0 3 6

Species
H
RM

relative
row min row max

Supplementary Figure 7 - Vectorial version of the heat map of metabolic changes to stored human and macaque RBCs

Species
Time (week)

Annotation
Maltose/Sucrose
D-Ribose
D-Glucose
1-4-beta-D-Xylan
Ascorbate
S-Adenosyl-L-methionine
5-Methylthioadenosine
L-aspartate
sn-glycero-3-Phosphoethanolamine
L-asparagine
Pyruvate
IMP
(S)(+)-Allantoin
UDP-glucose
AMP
D-Glyceraldehyde 3-phosphate/Glycerone phosphate
Inosine
Adenine
Adenine_SUPS
UDP-D-glucuronate
alpha-D-Ribose 1-phosphate
5-Phospho-alpha-D-ribose 1-diphosphate
ADP
2-3-Bisphosphoglycerate
D-Fructose 1-6-bisphosphate
ATP
5-6-Dihydrothymine
2/3-Phospho-D-glycerate
Phosphoenolpyruvate
Glycerol 3-phosphate
6-Phospho-D-gluconate
L-methionine
L-methionine_SUPS
L-glutamine_SUPS
Pyruvate_SUPS
D-Glucose_SUPS
D-Ribose_SUPS
1-4-beta-D-Xylan_SUPS
Maltose_SUPS
Glutathione
Cys-Gly
5-Hydroxyisourate
Urate
NADP+
2-3-Bisphosphoglycerate_SUPS
Phosphoenolpyruvate_SUPS
L-Citrulline
L-glutamine
3',5'-Cyclic AMP
UDP-N-acetyl-D-glucosamine
N-Acetylmethionine
D-Glyceraldehyde 3-phosphate/Glycerone phosphate_SUPS
UDP
ADP-D-ribose
(5-L-Glutamyl)-L-glutamine
Oxaloacetate
Citrate
Dehydroascorbate
N-Acetyl-L-ornithine
L-aspartate_SUPS
L-histidine
ATP_SUPS
ADP_SUPS
Adenosine_SUPS
Taurine
Tetradecenoic acid
Hexadecenoic acid
Adenosine
D-Hexose-phosphate
Putrescine
Spermidine
N1-Acetylspermine
(S)(+)-Allantoin_SUPS
S-Adenosyl-L-homocysteine
GMP
Hypoxanthine
Guanine
Guanine_SUPS
Inosine_SUPS
2-Oxoglutarate
L-glutamate
L-lysine
L-arginine
Asymmetric dimethyl arginine
Carnosine
IDP_SUPS
Ascorbate_SUPS
Glutathione disulfide
CMP-N-acetylneuraminate
Citrate_SUPS
D-Gluconate
gamma-L-Glutamyl-L-cysteine
(R)-S-Lactoylglutathione
S-Glutathionyl-L-cysteine
Hexadecanoic acid
Octadecanoic acid
L-cysteine
Succinate
Pentanoate (valerate)
Hexanoic acid (caproate)
Heptanoic acid
Octanoic acid (caprylate)
Nonanoic acid (pelargonate)
Decanoic acid (caprate)
L-arginine_SUPS
Tetradecanoic acid
Dodecanedioic acid
10-Hydroxydecanoic acid
Hexanoic acid (caproate)_SUPS
Heptanoic acid_SUPS
Octanoic acid (caprylate)_SUPS
Nonanoic acid (pelargonate)_SUPS
Decanoic acid (caprate)_SUPS
Tetradecanoic acid_SUPS
Dodecanedioic acid_SUPS
10-Hydroxydecanoic acid_SUPS
L-phenylalanine_SUPS
Hypoxanthine_SUPS
D-Hexose 6-phosphate_SUPS
Carnosine_SUPS
Dodecanoic acid_SUPS
L-glutamate_SUPS
2-Oxoglutarate_SUPS
Succinate_SUPS
Xanthine_SUPS
Octadecenoic acid
Octadecadienoic acid
Octadecatrienoic acid
Octadecenoic acid_SUPS
Linolate_SUPS
Octadecatrienoic acid_SUPS
(8Z-11Z-14Z)-Icosatrienoic acid_SUPS
Docosahexaenoic acid_SUPS
(7Z-10Z-13Z-16Z-19Z)-Docosa-7-10-13-16-19-pentaenoic acid_SUPS
Hexadecanoic acid_SUPS
Octadecanoic acid_SUPS
gamma-Glutamyl-Se-methylselenocysteine_SUPS
Tetradecenoic acid_SUPS
Hexadecenoic acid_SUPS
Taurine_SUPS
Spermine
Sphingosine 1-phosphate
Sphingosine 1-phosphate_SUPS
Guanidinoacetate
L-Citrulline_SUPS
glycine
NAD+
L-Homocysteine
L-valine
N-Methylethanolamine phosphate
L-leucine
L-leucine_SUPS
L-serine
Ornithine
D-Gluconic-1-5-lactone 6-phosphate
Sedoheptulose 1-phosphate
L-phenylalanine
L-tyrosine
L-tyrosine_SUPS
L-proline
L-proline_SUPS
L-alanine
L-threonine
Allantoate_SUPS
Ornithine_SUPS
L-threonine_SUPS
Oxaloacetate_SUPS
5-Hydroxyisourate_SUPS
Urate_SUPS
5-6-Dihydrothymine_SUPS
Cytidine
N1-Acetylspermidine
L-alanine_SUPS
Spermidine_SUPS
Spermine_SUPS
Mannitol/Sorbitol
UDP_SUPS
2-Hydroxyglutarate
Dodecanoic acid
Sphingosine
Lactate
Lactate_SUPS
L-histidine_SUPS
L-asparagine_SUPS
Allantoate
Fumarate
Malate
5-Oxoproline
5-Oxoproline_SUPS
Mannitol_SUPS
Fumarate_SUPS
Malate_SUPS
Cytidine_SUPS
L-lysine_SUPS
sn-glycero-3-Phosphoethanolamine_SUPS
Eicosatetraenoic acid
(8Z-11Z-14Z)-Icosatrienoic acid
Docosahexaenoic acid
(7Z-10Z-13Z-16Z-19Z)-Docosa-7-10-13-16-19-pentaenoic acid
Eicosapentaenoic acid
(5Z-8Z-11Z-14Z-17Z)-Icosapentaenoic acid
(5Z-8Z-11Z-14Z-17Z)-Icosapentaenoic acid_SUPS
Eicosatetraenoic acid_SUPS
L-valine_SUPS
N-Methylethanolamine phosphate_SUPS
L-cysteine_SUPS
L-cystine_SUPS
2-Hydroxyglutarate/Citramalate_SUPS
Dehydroascorbate_SUPS
L-serine_SUPS